ITER predictions using the GYRO verified and experimentally validated trapped gyro-Landau fluid transport model

2011 Nucl. Fusion 51 083001

(http://iopscience.iop.org/0029-5515/51/8/083001)

IOP Publishing and International Atomic Energy Agency Nuclear Fusion
Nucl. Fusion **51** (2011) 083001 (10pp) doi:10.1088/0029-5515/51/8/083001

ITER predictions using the GYRO verified and experimentally validated trapped gyro-Landau fluid transport model

J.E. Kinsey[1], **G.M. Staebler**[1], **J. Candy**[1], **R.E. Waltz**[1] and **R.V. Budny**[2]

[1] General Atomics, PO Box 85608, San Diego, CA 92186-5608, USA
[2] Princeton Plasmas Physics Laboratory, PO Box 451, Princeton, NJ 08543-0451, USA

E-mail: kinsey@fusion.gat.com

Received 25 January 2011, accepted for publication 27 May 2011
Published 23 June 2011
Online at stacks.iop.org/NF/51/083001

Abstract
The trapped gyro-Landau fluid (TGLF) transport model computes the quasilinear particle and energy driftwave fluxes in tokamaks with shaped geometry, finite aspect ratio and collisions. The TGLF particle and energy fluxes have been successfully *verified* against a large database of collisionless nonlinear gyrokinetic simulations using the GYRO code. Using a new collision model in TGLF, we find remarkable agreement between the TGLF quasilinear fluxes and 64 new GYRO nonlinear simulations with electron–ion collisions. In validating TGLF against DIII-D and JET H-mode and hybrid discharges we find the temperature and density profiles are in excellent agreement with the measured profiles. ITER projections using TGLF show that the fusion gains are somewhat more pessimistic than the previous GLF23 results primarily due to finite aspect ratio effects included only in TGLF. The synergistic effects of density peaking, finite β and $E \times B$ shear due to finite toroidal rotation lead to significant increases in fusion power above a reduced physics ITER base case. The TGLF results for ITER are confirmed using nonlinear GYRO simulations in place of TGLF to predict the temperature profiles within the TGYRO transport code. These results represent a snapshot of the ongoing effort to improve the TGLF model, validate it against experimental data, and make predictions for ITER.

(Some figures in this article are in colour only in the electronic version)

1. Introduction

It is commonly accepted that the standard model for most local cross-field transport losses in tokamaks is microturbulence due to drift waves including ion temperature gradient (ITG), trapped electron mode (TEM) and electron temperature gradient (ETG) modes. A new physics based driftwave model has been developed called the trapped gyro-Landau fluid (TGLF) model [1, 2]. TGLF is an eigenvalue code that solves a set of 15-moment GLF equations and includes the effects of shaped geometry via the Miller equilibrium model [3], trapped particle physics, collisions, $E \times B$ shear, and a wider spectrum than its predecessor (GLF23) [4] spanning from long wavelength ITG/TEM modes to short wavelength ETG modes. TGLF uses four Hermite basis functions, solving a 120×120 complex matrix to find the eigenvalues for each toroidal mode number. GLF23 uses a parametrized trial wave function and solves a much smaller 8×8 matrix for each low-k mode and a 4×4 matrix for each high-k mode. While GLF23 successfully reproduced the profiles from a wide variety of tokamak discharges [5], it assumed infinite aspect ratio shifted circle geometry. TGLF is the first comprehensive driftwave transport model valid for finite aspect ratio shaped geometry. The quasilinear transport fluxes are computed using a saturation rule that is local in wavenumber and uses the two most unstable linear eigenmodes for each wavenumber. TGLF is a local (spatially and in k-space) gyroBohm model. GyroBohm scaling is only broken by $E \times B$ shear effects in the saturation rule. The philosophy behind the development of TGLF has been to formulate a reduced gyro-Landau-fluid model that accurately describes the fundamental physics of turbulent driftwave transport and is well *verified* against linear and nonlinear gyrokinetic turbulence simulations. We find the TGLF quasilinear transport fluxes are a much better fit to nonlinear GYRO simulations than GLF23. To confidently predict the core confinement in ITER [6], we need

a comprehensive physics based model of turbulent transport that is also well *validated* against experimental data.

We first summarize the results of verifying TGLF against nonlinear GYRO [7, 8] simulations followed by the results of validating the model against experimental profile data including the DIII-D tokamak [9]. We then present the results from predictive modelling studies of ITER using TGLF and verification using GYRO. The effects of finite aspect ratio are found to have important consequences on the predicted fusion performance of ITER. An update of the TGLF collision model also has an impact on the predictions. Density peaking and finite β effects are both found to be beneficial. Since the predicted fusion performance is known to be sensitive to the temperature and density at the top of the H-mode pedestal we show the fusion predictions for ITER over a range in pedestal parameters. We also illustrate the consequences of stiff core transport on predicting the fusion gain first seen in [10] using the GLF23 model.

2. Verification of TGLF using GYRO nonlinear simulations

Model verification has played an essential role in the development of TGLF in an effort to accurately describe the linear growth rates and transport fluxes found in gyrokinetic turbulence simulations. We first used the GKS gyrokinetic stability code [11] to verify the linear growth rates and obtained an average root mean square (RMS) error of 11.4% for a database of 1799 linear growth rates [12]. The database is comprised of various parameter scans (k_y, a/L_n, a/L_T, q, $\hat{s}$, α, T_i/T_e, r/a and R/a) around three reference cases. The quasilinear saturation rule in TGLF was then determined using 82 nonlinear GYRO gyrokinetic simulations of ITG/TEM modes using Miller geometry [2]. The GYRO simulations were electrostatic, included kinetic electrons, and were performed with 16 toroidal modes with $0 \leqslant k_\theta \rho_s \leqslant 0.75$. The quasilinear saturation rule is local in space and k_y and uses the two most unstable linear eigenmodes. Comparing the TGLF quasilinear fluxes against the nonlinear fluxes from the GYRO transport database, remarkable agreement was obtained. While TGLF fits the GYRO simulations over a wide range of parameters we note that most of the cases are well above threshold. The GYRO simulations contain zonal flow and geodesic acoustic mode (GAM) physics and near threshold these effects can be important. TGLF does not explicitly contain zonal flow physics. In an effort to represent the effect of zonal flows in TGLF, the zonal flow damping rate (curvature drift frequency) was included in the nonlinear saturation rule (equation (3) in reference [2]). We do not expect TGLF to be accurate near threshold (in the absence of significant equilibrium $E \times B$ shear) where the $E \times B$ shearing from zonal flows can produce a nonlinear upshift in the critical gradient.

While the 82 GYRO simulations used to determine the TGLF saturation rule included shaped Miller geometry they did not include the effect of collisions. Recently, a new collision model was implemented in TGLF that was fit to numerical solutions of the gyrokinetic equation with pitch angle scattering of electrons [13]. TGLF with the new collision model (TGLF-09) was found to give much better agreement with GYRO collisional simulations. Comparing TGLF with

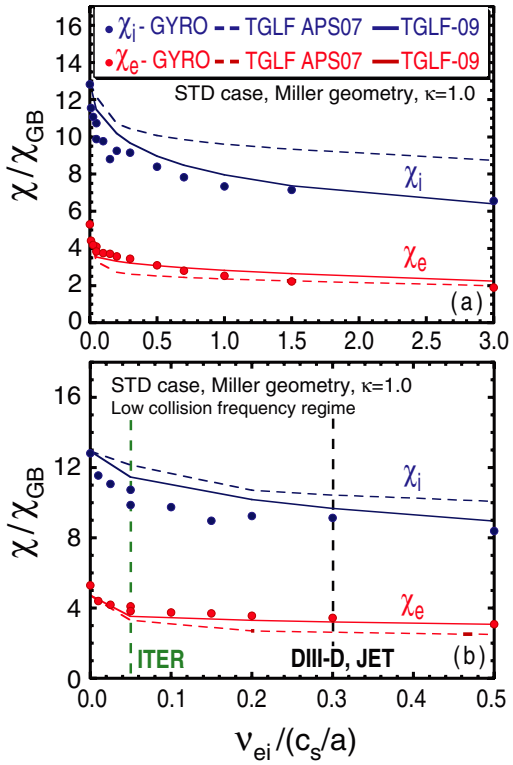

Figure 1. TGLF (solid, dashed lines) and GYRO (points) energy diffusivities versus $\nu_{ei}/(c_s/a)$ for the STD case with Miller geometry, $\kappa = 1.0$. Here, (a) shows the entire range of $\nu_{ei}/(c_s/a)$ studied and (b) focuses on the low $\nu_{ei}/(c_s/a)$ range. The vertical dashed lines denote the typical values for DIII-D, JET and ITER.

a new GYRO database of 64 collisional simulations, the average RMS errors in $[\chi_i, \chi_e]$ dropped from $[0.24, 0.27]$ to $[0.10, 0.13]$ going from the TGLF-APS07 model to the TGLF-09 model [14]. A description of the 64 simulations is given in table 1 of [14]. We define the RMS error as $\sigma_\chi = \sqrt{\sum \epsilon_j^2 / \sum \chi_{j,\mathrm{GYRO}}^2}$, where ϵ_j is the deviation between the TGLF and GYRO diffusivities. Here, the diffusivities are normalized to the gyroBohm diffusivity $\chi_{GB} = c_s \rho_s^2 / a$, where $c_s = \sqrt{T_e/m_i}$ is the ion sound speed, $\rho_s = c_s/\omega_{ci}$ is the ion gyroradius, $\omega_{ci} = eB_{unit}/(m_i c)$ is the ion cyclotron frequency, m_i is the ion mass, and $B_{unit} = (\rho/r)(\mathrm{d}\rho/\mathrm{d}r)B_0$ is the effective toroidal field [3, 15]. Figure 1 compares the TGLF and GYRO ion and electron energy diffusivities for a collision frequency scan around the GA standard (STD) case with Miller geometry, $\kappa = 1.0$, $\delta = 0.0$ and $k_\theta \rho_s \leqslant 0.75$. The top panel shows the diffusivities over the entire range studied while the bottom panel shows the results focusing on the low collision frequency region relevant to DIII-D, JET and ITER. The dashed lines denote the TGLF-APS07 results while the solid lines denote the TGLF-09 (new collision model) results. The vertical dashed lines denote the DIII-D, JET and ITER collision frequencies at the half radius. With finite levels of electron–ion collisions, the energy fluxes from TGLF-09 are lower for the ions and higher for the electrons compared with those from TGLF-APS07. Overall, TGLF-09 shows better agreement with GYRO. The GA standard case (STD) parameters with Miller geometry are $R/a = 3.0$, $r/a = 0.5$, $q = 2.0, \hat{s} = 1.0, \alpha = 0.0, \beta = 0.0, a/L_n = 1.0, a/L_T = 3.0$,

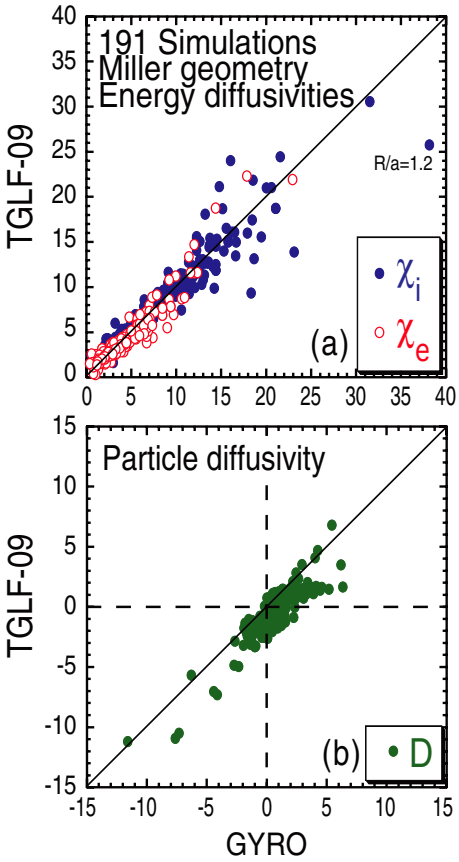

Figure 2. TGLF-09 versus GYRO (*a*) ion (blue) and electron (red) energy diffusivities and (*b*) particle diffusivity for 191 cases with Miller geometry.

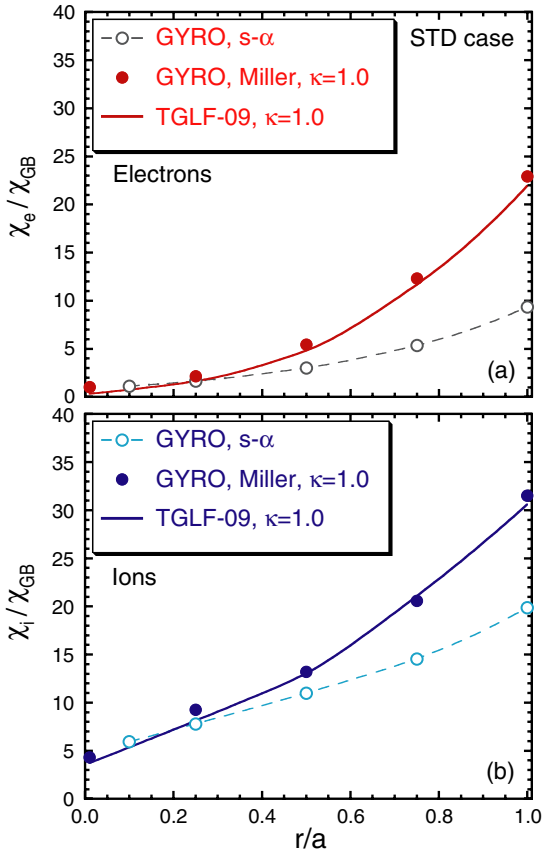

Figure 3. TGLF (solid lines) energy diffusivities and GYRO results (points) versus r/a for the STD case. The hollow points connected with dashed lines indicate the GYRO infinite aspect ratio $\hat{s}-\alpha$ results while the solid points indicate the results with Miller geometry, $\kappa = 1.0$, $s_\kappa = 0.0$ and $\delta = 0$.

$\nu_{ei}(a/c_s) = 0.0$, $T_i/T_e = 1.0$, $\kappa = 1.0$, $s_\kappa = (r/\kappa)\partial_r\kappa = 0.0$, $\delta = 0.0$, $s_\delta = [r/(1-\delta^2)^{1/2}]\partial_r\delta = 0.0$ and $\gamma_p(a/c_s) = 0.0$. Here, γ_p is the parallel velocity shear, ν_{ei} is the electron–ion collision frequency, $\hat{s} = (r/q)\mathrm{d}q/\mathrm{d}r$ is the magnetic shear, q is the local safety factor, $\alpha = -2R_o(q/B_o)^2(\mathrm{d}p/\mathrm{d}r)$ is the normalized pressure gradient, $\beta_e = n_eT_e/(B^2/8\pi)$ is the ratio of the electron plasma to magnetic field pressure, B is the toroidal magnetic field.

Figure 2 compares the energy and particle diffusivities from TGLF-09 against those in our GYRO transport database of 191 nonlinear simulations including the 64 recent cases with electron–ion collisions. All of the cases used Miller geometry and were electrostatic. The RMS errors averaged over the 11 scans with collisions in the database for $[\chi_i, \chi_e, D]$ are [0.13, 0.16, 0.78] for TGLF-09 compared with [0.24, 0.23, 0.98] for TGLF-APS07. While agreement with the GYRO energy diffusivities is quite good, obtaining good agreement with the GYRO particle diffusivities continues to be a challenge. Many of our cases are close to a null flow point which is especially challenging since some modes are driving an inward flow and some an outward flow. But, we note that updating the collision model in TGLF does lead to improved agreement of the particle transport with GYRO with the average RMS error in D for the 64 cases dropping from 0.98 to 0.78.

An important aspect of the TGLF model is that it is valid for finite aspect ratio shaped geometry through the use of the Miller equilibrium model [3]. While its predecessor, GLF23, was successful in reproducing the profiles from a wide variety of tokamak discharges [5], it was derived assuming infinite aspect ratio shifted circle geometry. GYRO simulations show that when the geometry is switched from $\hat{s}-\alpha$ to Miller equilibrium (with $\kappa = 1$) the finite aspect ratio in the Miller results in a significant increase in the energy transport especially for χ_e. GYRO results were first reported in [15]. Recent results by Burckel, Sauter *et al* also found the same effect [16]. The impact of finite aspect ratio on χ_e has important consequences on the predicted fusion performance of ITER. Figure 3 compares the time-averaged GYRO results (points) against the TGLF-09 results (solid lines) for a scan in r/a while holding all other parameters for the STD case fixed. As r/a increases, the trapped particle fraction increases and the difference between the $\hat{s}-\alpha$ and Miller diffusivities increases. TGLF-09 is able to reproduce this effect. In addition to finite aspect ratio effects, TGLF has also been successful in reproducing the stabilizing effect of elongation and elongation shear on ITG/TEM mode transport found in GYRO simulations [2, 15]. The effect of elongation also enters the model through the $E \times B$ shear quench rule. The quench rule is applied locally at each eigenmode $\gamma_{net} = \mathrm{Max}[(\gamma - \alpha_E\gamma_E), 0]$. Using a value of $\alpha_E = 0.3\sqrt{\kappa}$, a good fit to GYRO Miller geometry simulations for elongations of $\kappa = 1.0$, 1.5 and 2.0 was found.

3. Validation of TGLF: transport modelling of experimental profiles

The TGLF-09 model has been validated against a large profile database of 151 L- and H-mode discharges from the DIII-D, JET and TFTR tokamaks. Included are 25 DIII-D L-mode discharges (DB1), 40 DIII-D H-mode discharges (DB2), 30 DIII-D hybrid discharges (DB6), 8 DIII-D ITER Demo discharges (DB7), 28 JET H-mode discharges (DB4), 4 JET hybrid discharges and 16 TFTR L-mode discharges (DB9). We note that two of the DIII-D hybrid discharges have a similar ITER shape and were included in DB6 instead of DB7. The profile data for all JET and TFTR discharges and many of the DIII-D discharges were obtained from the ITER Profile Database [17, 18]. The rest of the DIII-D data were obtained by private means. We first examine the global figures of merit which include the average $\langle R_W \rangle$ and RMS error ΔR_W in the incremental stored energy (energy stored above the boundary condition) where

$$\langle R_W \rangle = \frac{1}{N} \sum_i (W_{si}/W_{xi}) \tag{1}$$

and

$$\Delta R_W = \sqrt{\frac{1}{N} \sum_i (W_{si}/W_{xi} - 1)^2}. \tag{2}$$

Here, i is the discharge index, N is the total number of discharges and $W_{s,x}$ refer to the simulation and experimental incremental stored energies, respectively. The incremental stored energy W_{inc} is given as

$$W_{inc} = \sum_{\hat{\rho}=0}^{\hat{\rho}_{BC}} [n_e T_e + n_i T_i] \, dV - \sum_{\hat{\rho}=0}^{\hat{\rho}_{BC}} \left[n_e T_{e,BC} + n_i T_{i,BC} \right] dV, \tag{3}$$

where $\hat{\rho}_{BC}$ is the radius of the boundary condition and T_{BC} is temperature evaluated at the boundary location. For all 151 discharges, the RMS error in the incremental stored energy W_{inc} (energy above the boundary location) is $\Delta R_W = 19\%$ for TGLF-09 which is lower than $\Delta R_W = 32\%$ obtained using GLF23. The effective offset for TGLF is $\langle R_W \rangle - 1 = 1\%$ while GLF23 has a value of $\langle R_W \rangle - 1 = -17\%$ (underpredicted). Figure 4 shows the predicted versus experimental W_{inc} using the TGLF-09 model. Examination of the local figures of merit (the RMS error σ_T and offset f_T) shows that TGLF-09 exhibits better agreement with the temperature profiles for all 151 discharges than GLF23. The average RMS errors in $[T_i, T_e]$ are [13%,15%] for TGLF-09 and [21%,23%] for GLF23. The average offsets are [0.002,0.006] for TGLF-09 and [−0.05,−0.10] for GLF23. Here, we predicted the temperature profiles using the XPTOR transport code with the same methodology described in [2]. The results for TGLF-APS07 are nearly identical to the TGLF-09 results because the change in the collision model mainly impacts the very low-k modes which tend to be quenched by $E \times B$ shear effects in most of discharges in the database. This is not found to be the case in our ITER predictions.

TGLF-09 has also been validated against recent DIII-D experiments designed to evaluate the four primary ITER operational scenarios incorporating the same shape and aspect ratio as ITER [19]. Overall, we find the level of agreement with the profiles from these ITER shaped discharges is as good as what was obtained in the 151 discharge database study. The one exception is discharge #133137 where TGLF-09 underpredicts both temperature profiles. Figure 5 shows the RMS errors (defined below) in the temperature profiles for 92 DIII-D and JET H-modes and hybrids in the top panel and 11 DIII-D ITER demo discharges in the bottom panel. The ITER demo database includes 8 discharges from DB7, two DIII-D hybrids with a similar ITER shape from DB2, and DIII-D ITER demo discharge #133137 which was not shown in figure 4. The horizontal dashed lines indicate the average RMS errors for $T_{e,i}$. Here, the four ITER scenarios include the baseline conventional edge-localized mode (ELM)y H-mode scenario, which targets $Q = 10$ at a plasma current of 15 MA the hybrid scenario, which targets high neutron fluence at a reduced current of 12.5 MA the steady-state scenario, which seeks fully noninductive operation at 9 MA with $Q \approx 5$; and the advanced inductive (AI) scenario which targets high fusion gain by optimizing high plasma current operation with increased magnetohydrodynamic (MHD) stability limits characteristic of hybrids.

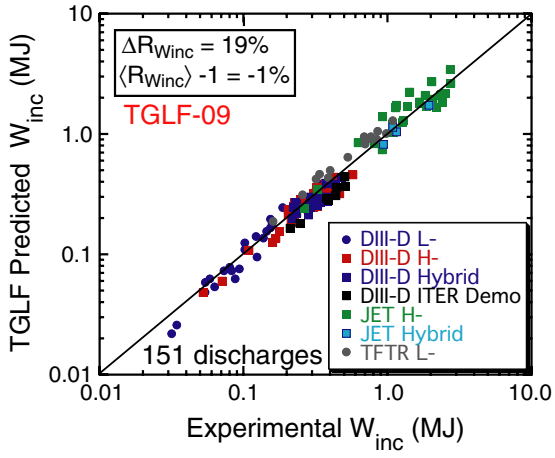

Figure 4. Predicted incremental stored energy W_{inc} from the TGLF-09 model versus experimental W_{inc} for 151 DIII-D, JET, and TFTR L-, H-mode, and hybrid discharges.

The RMS error σ_T and offset f_T between the predicted and experimental temperature profile for a given discharge are computed using the ITER Profile Database [17] definition,

$$\sigma_T = \sqrt{\frac{1}{N} \sum_j \epsilon_j^2} \Big/ \sqrt{\frac{1}{N} \sum_j T_{x,j}^2}$$

$$f_T = \frac{1}{N} \sum_{j=1}^{N} \epsilon_j \Big/ \sqrt{\frac{1}{N} \sum_j T_{x,j}^2},$$

where $\epsilon_j = T_{s,j} - T_{x,j}$ is the deviation between the jth radial simulation point $T_{s,j}$ and the corresponding experimental point $T_{x,j}$ and T is the local ion or electron temperature. The RMS error quantifies the scatter of the simulated profile about the experimental data normalized to an average value. The offset provides a measure of the amount by which the overall simulated profile needs to be shifted downwards (positive) or upwards (negative) in order to minimize σ_T. Both f_T and σ_T

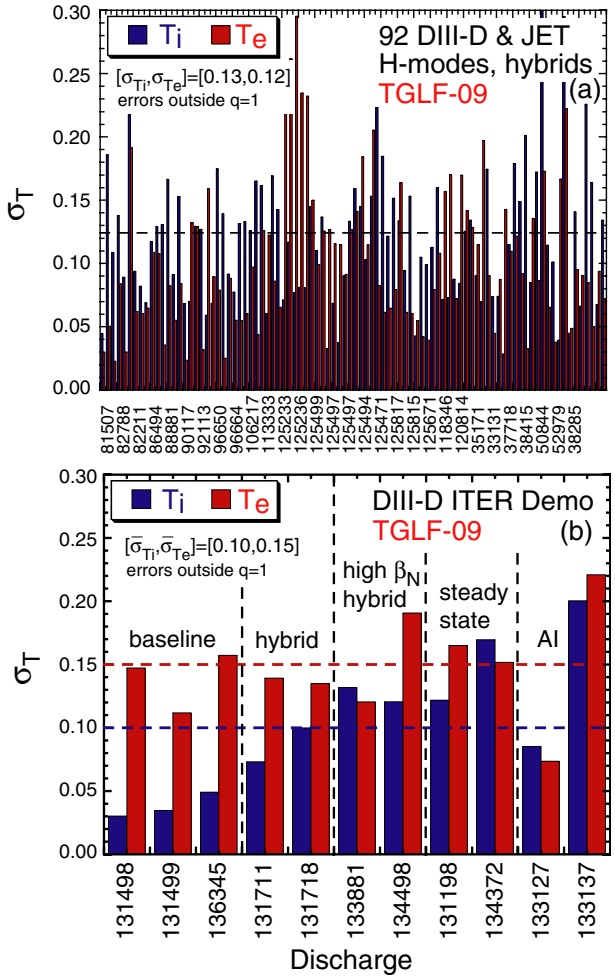

Figure 5. RMS error in T_i (blue) and T_e for 11 DIII-D ITER demo discharges using TGLF-09.

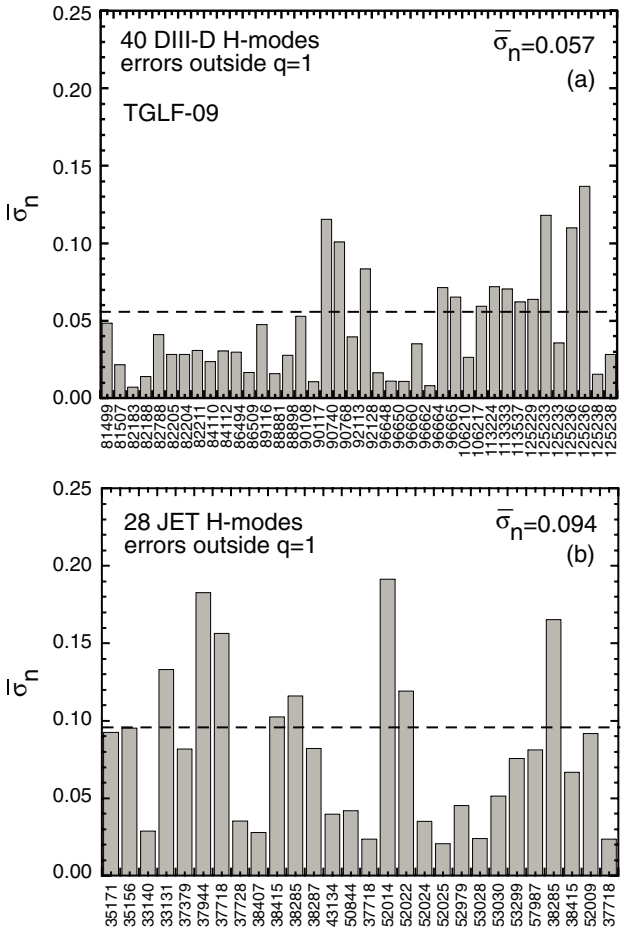

Figure 6. RMS error in n_e for (*a*) 40 DIII-D and (*b*) 28 JET H-mode discharges using TGLF-09. The dashed lines denote the average RMS error for the dataset.

are computed between the $q = 1$ radius (if present) and the boundary condition radius. The errors are not computed inside the $q = 1$ radius since this is not a true test of the transport models because of MHD sawtooth activity and time-averaging of the measured profiles across the sawteeth crashes.

In most of the discharges in the database we believe that $E \times B$ shear effects, which can increase the critical gradient, are large enough to dominate any missing zonal flow upshift effects in TGLF. In cases where $E \times B$ shear is small, any nonlinear upshift in the critical gradient is not being reproduced by TGLF. But, we believe this deficiency in the model is not a major concern if the upshift is not large and spatially localized. The stiff nature of the TGLF transport is forgiving in that the energy fluxes rise rapidly with temperature gradient such that the predicted temperature profiles would only mildly increase as a result of the critical gradient not being computed accurately. One caveat that is worth noting is that performing nonlinear simulations near threshold is very difficult and variations in the grid resolution can lead to noticeably different results.

3.1. Validation of particle transport

We find that TGLF reproduces the experimental density profiles for DIII-D and JET H-mode discharges as well as temperature profiles. The average RMS errors for n_e outside of $q = 1$ are $\sigma_n = 5.7\%$ and 9.4% for 40 DIII-D and 28 JET H-mode discharges, respectively. Here, we have taken the impurity and fast ion density profiles along with the beam and wall sources from experimental analyses. In the XPTOR simulations, a feedback mechanism is used whereby the wall source is scaled until a solution for the transport equations is obtained with a predicted electron density profile that matches the experimentally analysed line-averaged electron density. There is a great deal of uncertainty in the flux surface-averaged wall particle source. In our simulations, we take the particle source as computed in the ONETWO or TRANSP analysis code where some particle confinement time, which is largely unknown, was assumed. Therefore, we believe that some adjustment of the wall source is reasonable. Figure 6 show the RMS error for the electron density profile versus discharge for DIII-D and JET. The horizontal dashed line indicates the average σ_n for the dataset. The offset is not shown since we are forcing this to be approximately zero through the feedback method.

4. ITER predictions

The fusion performance has been assessed for the ITER 15 MA conventional ELMing H-mode scenario [6] using the TGLF

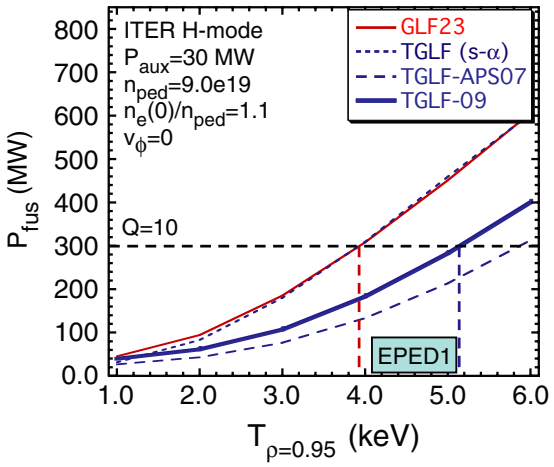

Figure 7. Predicted fusion power for a conventional H-mode ITER scenario with $P_{\rm aux} = 30$ MW and a prescribed density profile with $n_{e0}/n_{\rm ped} = 1.1$ ($\bar{n}_e/n_{\rm GW} = 0.8$) using the TGLF and GLF23 models.

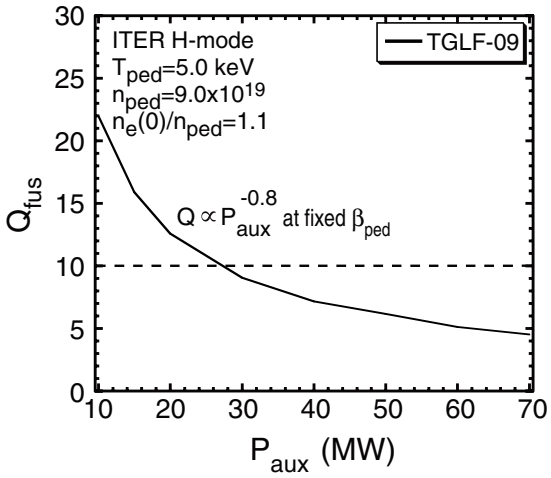

Figure 8. TGLF predicted fusion Q versus auxiliary heating power at fixed $\beta_{\rm ped,N} = 0.9$ for the reduced physics ITER case shown in figure 7. The dashed line denotes $Q = 10$.

and GLF23 models. The results presented in this paper are not intended to be taken as an optimization study. The TGLF predicted fusion power is more pessimistic than the GLF23 results primarily due to finite aspect ratio effects included only in TGLF. Figure 7 shows the predicted fusion power $P_{\rm fus}$ versus pedestal temperature ($T_{\rho=0.95}$) at fixed pedestal density using the TGLF and GLF23 models for an ITER conventional H-mode scenario with a somewhat flat prescribed density profile ($n_{e0}/n_{\rm ped} = 1.1$) and an auxiliary heating power of $P_{\rm aux} = 30$ MW (20 MW of ICRH and 10 MW of neutral beam injection (NBI)). The vertical dashed lines denote the pedestal temperatures yielding a target fusion gain of $Q = P_{\rm fus}/P_{\rm aux} = 10$. Using TGLF-09, the required value for $Q = 10$ is $T_{\rm ped} = 5.1$ keV corresponding to $\beta_{\rm ped,N} = 0.92$. The EPED model [20, 21] predicts a pedestal height under the boundary condition specified (two half widths in from the center of the edge barrier) in the range $\beta_{\rm ped,N} = 0.74$–0.92, depending on the input value of pedestal density and global β. By optimizing over these quantities, the value of $\beta_{\rm ped,N} = 0.92$ appears to be achievable. The ITER baseline parameters we used are $R = 6.2$ m, $a = 2.0$ m, $I_{\rm p} = 15$ MA, $B_{\rm T} = 5.3$ T, $\kappa = 1.75$, $Z_{\rm eff} = 1.7$, $M_{\rm i} = 2.5$, $v_\phi = 0$ for the toroidal rotation, and $n_{\rm ped} = 9 \times 10^{19}$ m^{-3} for the pedestal density.

Using infinite aspect ratio shifted circle geometry ($s - \alpha$), TGLF gives the same results as GLF23. When finite aspect ratio Miller geometry is used in TGLF, the ITG/TEM transport increases (mainly $\chi_{\rm e}$) causing the predicted $P_{\rm fus}$ to decrease (see the TGLF-APS07 results). Changes in the TGLF collision model also have an impact. Using the new collision model in TGLF (TGLF-09) results in an increase in $P_{\rm fus}$ relative to the TGLF-APS07 results but still below the GLF23 results. Above $T_{\rm ped} = 2$ keV, the TGLF-09 results scale like $T_{\rm ped}^2$ (or $\beta_{\rm ped}^2$) which is characteristic of a stiff transport model.

Stiff turbulent transport has important consequences on the fusion performance in ITER. Due to the stiff nature of TGLF, the temperature profiles are insensitive to changes in the amount of $P_{\rm aux}$ so that fusion Q scales like $1/P_{\rm aux}^{0.8}$ for a fixed $\beta_{\rm ped}$ as shown in figure 8. GLF23 was found to have a slightly stronger scaling of $1/P_{\rm aux}^{0.9}$ in [10]. Increasing $P_{\rm aux}$ while holding the $\beta_{\rm ped}$ fixed only slightly raises $P_{\rm fus}$ while reducing the fusion Q. Increasing the fusion power beyond the baseline prediction with additional $P_{\rm aux}$ is difficult. A positive consequence of stiff transport is that $P_{\rm aux}$ can be reduced with little decrease in $P_{\rm fus}$. Hence, increasing the fusion Q can be achieved by reducing $P_{\rm aux}$ while maintaining enough heating to remain above the H-mode power threshold.

Another consequence of stiff transport is that the profiles are relatively insensitive to changes in the auxiliary heating. We find the TGLF results are insensitive to varying mixtures of ICRH and NB heating while holding the total $P_{\rm aux}$ constant. For our ITER base case, we also find that the fusion projections are insensitive to reductions in the beam energy. Above $T_{\rm ped} = 2$ keV, changing the beam energy from 1 MeV to 250 keV in TRANSP results in only a 10% drop in the fusion power predicted by TGLF in XPTOR. Very little change (<5%) in the predicted density profile peaking is also observed. Hence, from a transport perspective, this suggests that 1 MeV beams may only be needed to achieve enough seed fusion power. Beyond that, neutral beams with lower energy may be sufficient but more studies are needed.

In our ITER modelling the $T_{\rm i}$ and $T_{\rm e}$ profiles are predicted taking the equilibrium, energy and particle sources and sinks from the output of a TRANSP simulation [22]. The density, fast ion and $Z_{\rm eff}$ profiles are held fixed and the toroidal rotation is assumed to be zero. The boundary conditions are enforced at a normalized toroidal flux of $\hat{\rho} = 0.95$ with $T_{\rm e,BC} = T_{\rm i,BC}$. When we reference $T_{\rm ped}$ we are referring to the $\hat{\rho} = 0.95$ location. The predicted temperatures are evolved to a steady-state solution of the transport equations using a fully implicit Newton solver in the XPTOR transport code. The fusion power, ohmic heating, bremsstrahlung and synchrotron radiative losses are computed self-consistently assuming an effective main ion mass of $A = 2.5$ (50–50 DT ion mixture) and a single carbon impurity species. The effect of helium ash accumulation was not considered.

4.1. Sensitivity to ETG modes

Recent TGLF modelling studies have shown that ETG transport can dominate the electron energy transport in DIII-D

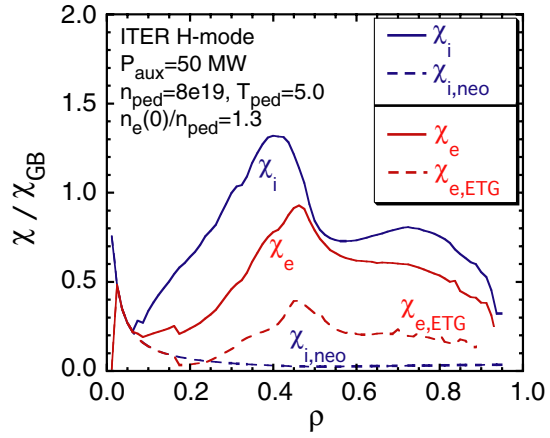

Figure 9. TGLF-09 ion (blue) and electron (red) energy diffusivities versus $\hat{\rho}$ for the ITER ELMy H-mode scenario with $\beta_{\mathrm{ped,N}} = 0.9$. The dashed red and blue lines denotes the high-k part of χ_e/χ_{GB} and the neoclassical energy diffusivity, respectively.

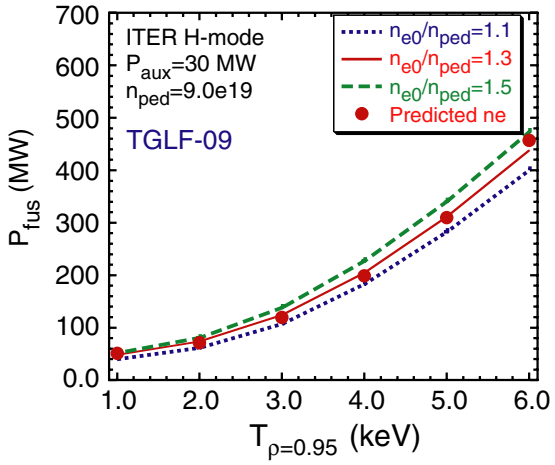

Figure 10. TGLF predicted fusion power versus T_{ped} for various density peaking factors for the ITER scenario with 30 MW of auxiliary heating. The lines denote the results with a prescribed density profile and the points indicate the results where the density profile was predicted along with T_e and T_i.

hybrid discharges where $E \times B$ shear effects have quenched the low-k modes [14]. But, there is some uncertainty in how large the high-k saturation levels should be in TGLF when Miller geometry is used. The ETG contribution to χ_e in TGLF (above $k_\theta \rho_s = 1.0$) was calibrated to yield a ratio of $\chi_{\text{high-}k}/\chi_{\text{e,low-}k} \simeq 0.12$ to match a single coupled low/high-k GYRO simulation of the GA-STD case assuming shifted circle geometry and a reduced mass ratio of $\mu = \sqrt{m_i/m_e} = 30$ [2, 23]. Comparable coupled low/high-k GYRO nonlinear simulations with Miller geometry have yet to be performed.

The predicted fusion power in ITER is found to be relatively insensitive to the ETG transport levels in TGLF. Several reference H-mode cases were considered where the ETG transport was eliminated from the TGLF spectrum. Figure 9 shows the predicted TGLF energy diffusivities for the case with $P_{\mathrm{aux}} = 50\,\mathrm{MW}$, $n_{e0}/n_{\mathrm{ped}} = 1.3$, $T_{\mathrm{ped}} = 5.0\,\mathrm{keV}$ and $n_{\mathrm{ped}} = 8.0 \times 10^{19}\,\mathrm{m}^{-3}$. Here, the ETG modes contribute approximately 30% to the total χ_e. On average, P_{fus} increases by only ≈5% when ETG modes are removed from the TGLF spectrum compared with the baseline result with ETG modes. As the ETG transport is reduced, the temperature gradients increase making the ITG/TEM modes more unstable. As a result, there is very little decrease in the total energy transport when the mixture of low/high-k mode is varied. Since $E \times B$ shear effects are likely to be weak in ITER without external torque, it would appear that the accuracy of ETG transport is not important.

4.2. Sensitivity to density peaking

At fixed β_{ped}, we find moderate density peaking improves ITER performance by about 5% above the baseline case with a flat density profile. While we have not considered impurity and/or helium ash accumulation, a higher reactivity is evident and fairly robust. Figure 10 shows the fusion power versus T_{ped} for three different prescribed n_e profiles (lines) with varying density peaking factors. TGLF predictions of the density profile (red dots) yields peaking factors of $n_{e0}/n_{\mathrm{ped}} = 1.3$ fairly robustly over the entire range of T_{ped} values. This is consistent with the peaked density profiles with $n_{e0}/n_{\mathrm{ped}} \geqslant 1.3$ have been observed in low collisionality AUG, JET and C-Mod H-mode plasmas [24–27]. Here, we used the fast ion density and Z_{eff} profiles from TRANSP and predicted the electron density along with the ion and electron temperatures using TGLF in XPTOR.

4.3. Sensitivity to finite β, and finite toroidal rotation

Including finite β (i.e. electromagnetic) effects in TGLF also leads to a 5% increase in P_{fus} above the ITER baseline case. In low to moderate β_N DIII-D and JET cases we have found finite β effects to be mildly stabilizing. However, recent studies of DIII-D hybrids with $\beta_N \geqslant 3$ have shown a stronger stabilizing effect [14]. This could be beneficial in 12 MA ITER hybrids operating at lower densities than the 15 MA conventional ELMy H-mode scenarios. Using the toroidal rotation profile, as predicted by TRANSP in [22], also produces a 5% increase in P_{fus} due to $E \times B$ shear stabilization. The toroidal rotation peaked at $4 \times 10^4\,\mathrm{m\,s}^{-1}$ and was obtained in a predictive TRANSP run setting $\chi_\phi = \chi_i$, where GLF23 was used for the energy transport. Figure 11 shows the TRANSP toroidal rotation (and safety factor) profile used in our simulations.

4.4. Synergistic effects on predicted fusion power

While the individual benefits of density peaking, finite β and $E \times B$ shear from small toroidal rotation v_ϕ are not large, the combined synergistic increase in P_{fus} is ≈60% above the conservative base case with 285 MW. Table 1 summarizes the results of including density peaking, finite β and finite v_ϕ for the $T_{\mathrm{ped}} = 5.0\,\mathrm{keV}$ case shown in figure 3 using TGLF-09. The value of $\beta_{\mathrm{ped,N}} = 0.9$ needed for the case in table 1 is within the range of predictions by the EPED pedestal model. With moderate density peaking finite β effects yield a 20% increase in the predicted fusion power above the electrostatic case. Here, the central T_e and T_i values increase by 11%. While TGLF modelling of other ITER H-mode and hybrid cases have shown similar results more detailed studies are needed in order to assess the robustness of the effect and identify the

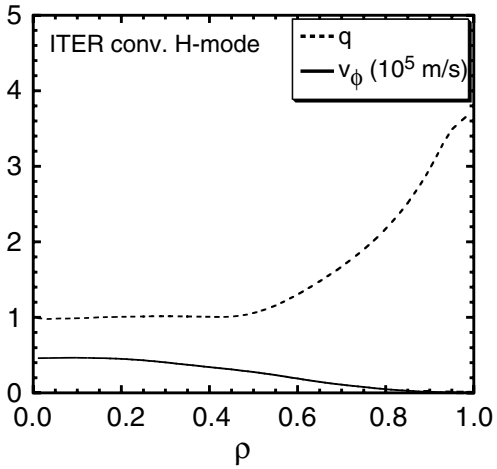

Figure 11. TRANSP toroidal rotation and safety factor profiles used in the simulations of the ITER baseline H-mode scenario.

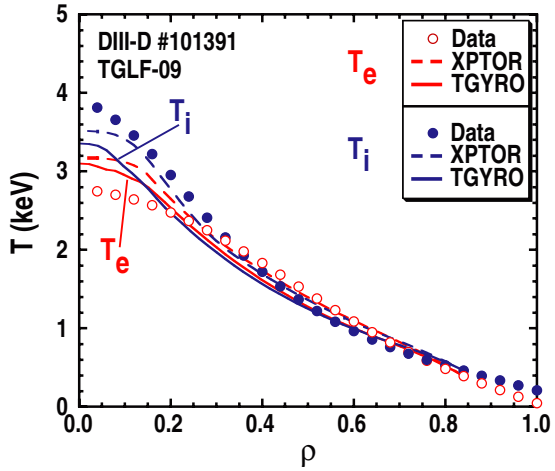

Figure 12. TGLF-09 predicted temperatures for DIII-D #101391 using the XPTOR (dashed lines) and TGYRO (solid lines) codes.

Table 1. ITER performance using TGLF-09 for a conventional H-mode scenario with $P_{\rm aux} = 30$ MW, $v_\phi = 0$, $n_{\rm e0}/n_{\rm ped} = 1.1$, $T_{\rm ped} = 5.0$ keV, $n_{\rm ped} = 9.0 \times 10^{19}$ m^{-3}, $\beta_{\rm ped,N} = 0.9$.

Scenario variation	$P_{\rm fus}$ (MW)
Base case with prescribed $n_{\rm e}$ ($n_{\rm e0}/n_{\rm ped} = 1.1$)	285
Predicted density with $n_{\rm e0}/n_{\rm ped} = 1.3$	310
Finite β with prescribed $n_{\rm e}$ ($n_{\rm e0}/n_{\rm ped} = 1.1$)	311
Predicted $n_{\rm e0}/n_{\rm ped} = 1.3$, finite β	373
Predicted $n_{\rm e0}/n_{\rm ped} = 1.3$, finite β, $v_{\phi,0} = 0.5 \times 10^5$ (m s^{-1})	452

conditions where finite β become important. It is curious that previous modelling of DIII-D β scans have shown very little β dependence in the local core transport (even with finite β effects included) and yet in ITER finite β effects appear to play more of a role. In general, there is a need to study and validate electromagnetic effects for ITER-like conditions in addition to being able to confidently predict the momentum transport. We note that with the three ingredients and $\beta_{\rm ped,N} = 0.92$, increasing $P_{\rm aux}$ from 30 MW to 44 MW results in 500 MW of fusion power. At the lower end of $\beta_{\rm ped,N} = 0.74$, increasing $P_{\rm aux}$ 30 to 56 MW results in 400 MW of fusion power.

4.5. Verification of the TGLF ITER results against GYRO using TGYRO

The TGYRO framework [28] has been used as an additional tool for verifying the XPTOR/TGLF results. Our goal is to verify the TGLF ITER predictions obtained using the XPTOR code against TGYRO predictions using local GYRO flux tube simulations to compute the turbulent energy transport. TGYRO is a steady-state transport code which adjusts temperature, density and toroidal rotation profiles until the simulated flows match input source flows from the plasma centre to the pedestal. TGYRO can use either GYRO or TGLF to compute turbulent fluxes, thus providing a unified framework for TGLF-GYRO verification and validation of both with experimental data. TGYRO can also call the NEO code to compute self-consistent, first-principles neoclassical fluxes, poloidal flows and bootstrap current in general geometry [29].

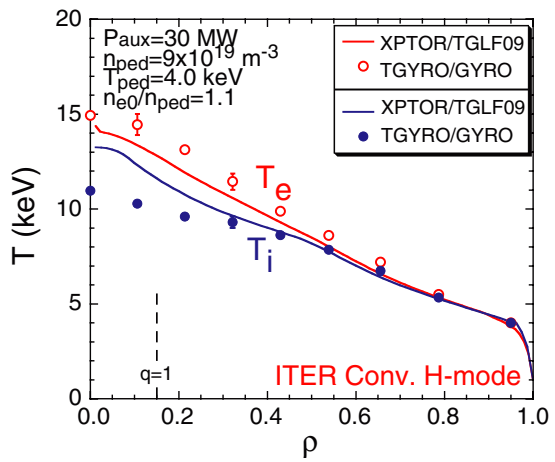

Figure 13. Predicted temperatures for an ITER H-mode scenario with no dilution using XPTOR/TGLF-09 and TGYRO/GYRO. The lines denote the TGLF results and the points denote the GYRO results.

The results of code benchmarking TGYRO against XPTOR using TGLF-09 for a DIII-D L-mode are shown in figure 12. The agreement is excellent for the temperature profile predictions including the effects of $E \times B$ shear and assuming no dilution. However, differences are apparent in the central core region. Here, neoclassical transport is the dominant loss mechanism. Differences in the neoclassical transport in the XPTOR and TGYRO codes contribute to the differences in the predicted temperatures inside $\hat{\rho} = 0.2$. Figure 13 shows the TGYRO/GYRO results compared with the XPTOR/TGLF-09 results for the conservative ITER base case shown in figure 7 with $T_{\rm ped} = 4.0$ keV and no dilution. In TGYRO, GYRO flux tube simulations were performed at eight radial zones with eight toroidal modes, $\hat{k}_y \leqslant 0.70$, and a box size of $[L_x/\rho_{\rm s}, L_y/\rho_{\rm s}] = [64, 64]$. The GYRO results are in good agreement with the TGLF-09 results, thus providing confidence in our ITER predictions. However, we note that the TGYRO/GYRO results are not well converged in the central core region $\hat{\rho} \leqslant 0.3$ where the profiles reside very close to threshold and the transport is bursty and not well saturated. The error bars indicate one standard deviation in the time

variation of the GYRO results. A nonlinear upshift in the critical gradient due to zonal flows is observed in the GYRO simulations for these ITER parameters. TGLF does not include any model for the zonal flows, so the TGLF predictions may be a bit pessimistic. While equilbrium $E \times B$ shear effects may have masked the nonlinear upshift effects of zonal flows in DIII-D and JET, that is not the case in ITER where $E \times B$ shear effects are smaller. In addition to zonal flows, we have shown that other small effects can synergistically reduce the energy transport such that significant increases in the predicted fusion power are observed. More detailed studies of these effects, including zonal flows, are needed for near threshold conditions.

5. Quantifying and assessing the local stiffness of TGLF

While there is an ongoing debate about exactly how stiff experimental temperature profiles are in existing devices, there are numerous published examples citing empirical evidence from various tokamaks of critical temperature gradient behaviour. In particular, results published by Baker *et al* [30] showed that χ_i from experimental analyses of DIII-D L-mode rises rapidly above some threshold value of R/L_T. Analyses of AUG data by Ryter *et al* [31, 32] are consistent with the assumption that temperature profiles are limited by a critical gradient length with the T_e profiles exhibiting a stiff response to changes in auxiliary heating. Supporting evidence for a critical T_e gradient in Tore Supra has been reported by Hoang *et al* in [33]. Recent analysis of JET experiments shows evidence of core ion stiffness and that it can be reduced with increasing shear in the toroidal rotation [34]. TGLF modelling was able to reproduce this effect. Since stiff energy transport has a significant impact on the predicted ITER performance in our simulations it is important to quantify the level of stiffness from TGLF and assess how ITER compares with discharges from existing tokamaks.

Here, we increased a/L_T for both the ions and electrons by 10% at the last call of the transport run where a solution has been obtained for the steady-state profiles. The combined core stiffness is defined in terms of changes in the total transport power in response to changes in the temperature gradient scale lengths,

$$S_{tr} = \frac{\partial \ln P_{tr}}{\partial \ln z} = \frac{\Delta(P_{tr,e} + P_{tr,i})/(P_{tr,e} + P_{tr,i})}{0.5\left[\Delta(a/L_{T_i})/(a/L_{T_i}) + \Delta(a/L_{T_e})/(a/L_{T_e})\right]}, \quad (4)$$

where $z = -1/L_T = -\mathrm{d}\ln T/\mathrm{d}r = -(1/T)(\mathrm{d}T/\mathrm{d}r)$, $P_{tr} = -V' n \chi \partial T/\partial r$ is the TGLF predicted transport power flow, a/L_T is the temperature gradient scale length, $\Delta(a/L_T) = 0.10$ is the variation in a/L_T for both the electrons and ions, $V' = \mathrm{d}V/\mathrm{d}r$, and χ is the effective energy diffusivity. The stiffness in GYRO simulations of a DIII-D discharge has been previously quantified in terms of the effective energy diffusivity in response to changes in a/L_{T_i} in [35].

For the conventional H-mode scenario we find that the temperature profile stiffness in ITER is comparable to what is found in DIII-D and JET. Figure 14 shows the stiffness S versus $\hat{\rho}$ for two typical DIII-D and JET H-mode cases compared with the ITER three-ingredient conventional H-mode case with $\beta_{ped,N} = 0.9$. Here, we examined a dozen or so DIII-D and JET H-mode cases and compared the local stiffness in the energy transport power flow with that from our conventional H-mode ITER case. We also find the stiffness decreases with increasing radius beyond $\hat{\rho} = 0.5$ as the profiles rise increasingly above threshold and the transport spectrum becomes more TEM dominant. Closer to the marginal point (i.e. $\hat{\rho} = 0.4$) the stiffness is larger than at larger radii. For the DIII-D and JET cases shown, S is approximately two times larger than what is found near the boundary location (near $\hat{\rho} = 0.8$). In DIII-D, the stiffness also decreases with increasing toroidal rotation in qualitative agreement with the JET results reported in [34] where TGLF demonstrated a significant change in the stiffness due to changes in rotation near threshold. Here, we caution the reader in that only two discharges have been analysed, so the robustness of the result is unclear.

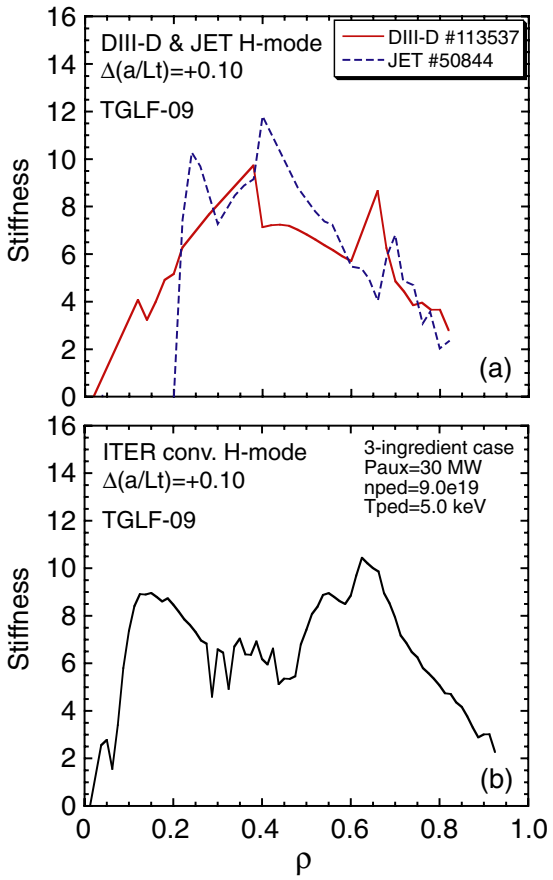

Figure 14. Stiffness S profiles for H-mode discharges (a) DIII-D #113537 and JET #50844 compared with (b) the ITER conventional H-mode three-ingredient case with predicted density, finite β and finite toroidal rotation.

6. Summary

The results can be summarized as follows:

(i) TGLF has been verified against 191 nonlinear GYRO simulations. The database RMS errors for [χ_i, χ_e, D] are [0.13, 0.16, 0.78] for TGLF-09 (with the new collision model) compared with [0.24, 0.23, 0.98] for TGLF-APS07 (with the old collision model).

(ii) TGLF accurately predicts both the electron and ion temperature profiles with average RMS values in $[T_i, T_e]$ of [13%,15%] for 151 L- and H-mode discharges from DIII-D, JET and TFTR. GLF23 has RMS errors of [21%,23%].

(iii) Finite aspect ratio effects in TGLF (Miller geometry) cause the fusion projections in ITER to be lower than that for GLF23 (infinite aspect ratio, shifted circle geometry).

(iv) Because of the stiff transport properties of TGLF, the fusion Q scales like β_{ped}^2 and also like $P_{aux}^{-0.8}$ at fixed pedestal β (a perfectly stiff core scales like $Q \propto P_{aux}^{-1}$).

(v) For small levels of $E \times B$ shear, the fusion power in ITER is sensitive to the choice of collision model in TGLF. Improving the collision model in TGLF raises the predicted fusion power compared with the TGLF-APS07 results.

(vi) Three ingredients for improving ITER performance have been identified including density peaking, finite β and $E \times B$ shear due to some finite toroidal rotation. Each improves P_{fus} by 5%. Combined, they produce close to a 60% increase in P_{fus} above the conservative baseline case to yield $Q = 15$ and $P_{fusion} = 452$ MW at $\beta_{ped,N} = 0.9$ (table 1).

(vii) The XPTOR/TGLF-09 results for ITER have been verified against the TGYRO code using GYRO nonlinear simulations for the energy transport.

(viii) For the conventional H-mode scenario, the temperature profile stiffness in ITER is comparable to what is found in DIII-D and JET. The core stiffness has been quantified with typical values in the range $S = 5$–10.

(ix) The predictions in this paper are not the result of an optimization study of ITER and represent a snapshot of the ongoing effort to improve the TGLF model, validate it against experimental data, and make predictions for ITER.

In future work, there is a need to compare TGLF against nonlinear GYRO simulations with moderate to large values of β and shaped geometry. The impact of electromagnetic effects on both the low-k and high-k modes needs to be examined especially for core plasma conditions with moderate to high-β values. We also plan on implementing momentum transport in TGLF and validating the predicted toroidal rotation profiles against experimental data. Historically, the focus has been on developing and testing core turbulence models. The results found here for DIII-D hybrids demonstrate the need to also develop improved models for neoclassical transport. We plan to implement the NEO code into the XPTOR transport code to be used in conjunction with the TGLF model.

Acknowledgments

This work was supported by the US Department of Energy under DE-FG03-95ER54309, DE-FG03-92ER54141 and DE-AC02-09CH11466. We thank the DIII-D and JET experimental teams for providing the profile data. The GYRO simulations were made possible through generous allotments of computer time at NERSC and ORNL.

References

[1] Staebler G.M., Kinsey J.E. and Waltz R.E. 2007 *Phys. Plasmas* **14** 055909
[2] Kinsey J.E., Staebler G.M. and Waltz R.E. 2008 *Phys. Plasmas* **15** 055908
[3] Waltz R.E. and Miller R.L. 1999 *Phys. Plasmas* **6** 4265
[4] Waltz R.E., Staebler G.M., Dorland W., Hammett G.W., Kotschenreuther M. and Konings J.A. 1997 *Phys. Plasmas* **4** 2482
[5] Kinsey J.E. 2005 *Fusion Sci. Technol.* **48** 1060
[6] Shimada M. *et al* 2007 *Nucl. Fusion* **47** S1
[7] Candy J. and Waltz R.E. 2003 *J. Comput. Phys.* **186** 545
[8] Candy J. and Waltz R.E. 2003 *Phys. Rev. Lett.* **91** 45001
[9] Mahdavi A. and Luxon J.L. 2005 *Fusion Sci. Technol.* **48** 2
[10] Kinsey J.E., Bateman G., Onjun T., Kritz A.H., Staebler G.M. and Waltz R.E. 2003 *Nucl. Fusion* **43** 1845
[11] Kotschenreuther M., Rewoldt G. and Tang W.M. 1995 *Comput. Phys. Commun.* **88** 128
[12] Staebler G.M., Kinsey J.E. and Waltz R.E. 2005 *Phys. Plasmas* **12** 102508
[13] Staebler G.M. and Kinsey J.E. 2010 *Phys. Plasmas* **17** 1
[14] Kinsey J.E., Staebler G.M. and Petty C.C. 2010 *Phys. Plasmas* **17** 122315
[15] Kinsey J.E., Waltz R.E. and Candy J. 2007 *Phys. Plasmas* **14** 102306
[16] Burckel A., Sauter O., Angioni C., Candy J., Fable E. and Lapillonne X. 2010 *J. Phys.: Conf. Ser.* **260** 012006
[17] ITER Physics Expert Groups on Confinement and Transport and Confinement Modeling and Database 2000 *Nucl. Fusion* **40** 1955
[18] Roach C. *et al* 2008 *Nucl. Fusion* **48** 125001
[19] Doyle E.J. *et al* 2010 *Nucl. Fusion* **50** 075005
[20] Snyder P.B., Groebner R.J., Leonard A.W. and Osborne T.H. 2009 *Phys. Plasmas* **16** 056118
[21] Snyder P.B. *et al* 2010 *23rd IAEA Fusion Energy Conf. (Daejeon, South Korea, 11–16 October 2010)* (Vienna: IAEA) CD-ROM file THS/1-1 and http://www-naweb.iaea.org/napc/physics/FEC/FEC2010/html/index.htm
[22] Budny R.V. 2009 *Nucl. Fusion* **49** 085008
[23] Waltz R.E., Candy J. and Fahey M. 2007 *Phys. Plasmas* **14** 056116
[24] Valovic M. *et al* 2004 *Plasma Phys. Control. Fusion* **46** 1877
[25] Weisen H. *et al* 2005 *Nucl. Fusion* **45** L1
[26] Angioni C. *et al* 2007 *Nucl. Fusion* **47** 1326
[27] Greenwald M., Angioni C., Hughes J.W., Terry J. and Weisen H. 2007 *Nucl. Fusion* **47** L26
[28] Candy J., Holland C., Waltz R.E., Fahey M.R. and Belli E. 2009 *Phys. Plasmas* **16** 060704
[29] Belli E. and Candy J. 2008 *Plasma Phys. Control. Fusion* **50** 095010
[30] Baker D.R. *et al* 2001 *Phys. Plasmas* **8** 4128
[31] Ryter F., Leuterer F., Pereverzev G., Fahrbach H.U., Suttrop W. and the ASDEX Upgrade Team 2001 *Phys. Rev. Lett.* **86** 2325
[32] Ryter F., Angioni C., Peeters A.G., Leuterer F., Fahrbach H.U., Suttrop W. and the ASDEX Upgrade Team 2005 *Phys. Rev. Lett.* **95** 085001
[33] Hoang, G.T., Bourdelle C., Garbet X., Giruzzi G., Aniel T., Ottavani M., Horton W., Zhu P. and Budny R.V. 2001 *Phys. Rev. Lett.* **87** 125001
[34] Mantica P. *et al* 2010 *23rd IAEA Fusion Energy Conf. (Daejeon, South Korea, 11–16 October 2010)* (Vienna: IAEA) CD-ROM file EXC/9-2 and http://www-naweb.iaea.org/napc/physics/FEC/FEC2010/html/index.htm
[35] Waltz R.E., Candy J., and Petty C.C. 2006 *Phys. Plasmas* **13** 072304